NASA Technical Memorandum 4039

Three-Dimensional Models of Conventional and Vertical Junction Laser-Photovoltaic Energy Converters

John H. Heinbockel and Gilbert H. Walker

JULY 1988

NASA

NASA Technical Memorandum 4039

Three-Dimensional Models of Conventional and Vertical Junction Laser-Photovoltaic Energy Converters

John H. Heinbockel
Old Dominion University
Norfolk, Virginia

Gilbert H. Walker
Langley Research Center
Hampton, Virginia

National Aeronautics
and Space Administration

**Scientific and Technical
Information Division**

1988

Symbols

a, b	x and y half-width dimensions, cm
$B(\,)$	boundary operator
D_n, D_p	diffusion coefficients of electrons and holes, cm^2-s^{-1}
G_1, G_2, g_1, g_2	Green's functions
g	generation rate, photons/cm^3-s
H	depth of planar cell, cm
$H(\,)$	partial differential operator
h'	depth parameter, $H - z_j - w$, cm
I_{sc}, I_d	currents, A
J_n, J_p, J_0	current density of electrons and holes, A-cm^{-2}
J_{pd}, J_{nd}	dark current density, A-cm^{-2}
J_{sc}	short circuit current density, A-cm^{-2}
$L(\,)$	linear differential operator
L_n, L_p	diffusion lengths of electrons and holes, cm^2-s^{-1}
n_p, p_n, n_{p0}, p_{n0}	densities of electrons and holes, cm^{-3}
R	reflection coefficient, dimensionless
R_n, R_p	regions n and p
R_s	series resistance, ohms
R_{sh}	shunt resistance, ohms
S, S_I, S_n, S_p	surface recombination velocities, cm-s^{-1}
U_m, V_m, U_m^*, V_m^*	eigenfunctions
x, y, z	coordinates
z_j	junction depth, cm
α	absorption coefficient, cm^{-1}
η_i, η_i^*	eigenvalues
ϕ_0	rate of incident photons, cm^{-2}-s^{-1}
ω	width of depletion region, cm

Summary

In order to achieve a better understanding and comparison of conventional and vertical junction laser-photovoltaic energy converters, we have constructed three-dimensional analytical models of their operation. These models simulate the conversion of laser power into electrical power and are constructed for both planar conventional and vertical junction photoconverters. The models are a set of linear partial differential equations and take into account many photoconverter design parameters. From the models, we extract the spectral response and current-voltage relations from solutions to the partial differential operators in terms of Green's functions. The model is applied to Si photoconverters; however, the model may be used with other semiconductors. The conversion efficiency of the Si vertical junction photoconverter is 47 percent, whereas the efficiency for the conventional Si planar device is only 17 percent. A parametric study of the vertical junction Si converter is then done in order to describe the optimum converter for use with a 1.06-μm Nd laser. The optimum Si vertical junction converter for a single junction is 1 mm deep by 1 cm wide by 0.035 mm thick. The junction is located 2 μm from one edge. The doping density for both acceptors and donors is 1×10^{18} cm^{-3}. A reflectivity of 5 percent is assumed. The efficiency for this optimized vertical junction converter is 44 percent at 1 kW-cm^{-2}.

Introduction

Photovoltaic converters have many applications for satellite and space station power needs. In this paper, we are concerned with the application of photovoltaics for the conversion of laser power to electrical power in a space-based laser power system (ref. 1). We envision laser radiation on the order of 1.0 kW-cm^{-2} (ref. 1) at a specific wavelength that depends upon the type of laser considered. Semiconductors for use as laser power converters must be chosen such that their bandgap energy is less than the energy of the laser photons (ref. 2). In this study, we develop three-dimensional analytical models to compare planar conventional photoconverters with vertical junction photoconverters in order to achieve a comparison of how these energy converters operate. The photoconverter considered is Si which has a bandgap energy of 1.11 eV. For this type of photoconverter, we consider a Nd laser which emits 1.06 μm radiation which is near the Si bandgap. The models for the conversion of laser power to electrical power are based upon a set of linear partial differential equations with appropriate boundary conditions. Solutions of these equations are obtained in terms of Green's functions (ref. 3) for the regions n and p. From these solutions, various output quantities are calculated. In particular, we calculate the efficiencies of the converters, the spectral response, current voltage relationships, and contour plots of the current density at the junction edge. Temperature gradients are neglected. The method used is very general and will handle a wide variety of source terms.

Model

General

The geometry for the three-dimensional models of an n/p photoconverter is illustrated in figure 1. We denote the region n by

$$R_n = \{x, y, z \quad | \quad |x| \leq a, \ |y| \leq b, \ 0 \leq z \leq z_j\}$$

and denote the region p by

$$R_p = \{x, y, z \quad | \quad |x| \leq a, \ |y| \leq b, \ z_j + \omega \leq z \leq H\}$$

The junction doping is assumed to be linear and abrupt at the junction edge. For the planar conventional photoconverter, we let

$$g(z) = \phi_0(1 - R)\alpha \exp(-\alpha z) \tag{1}$$

denote the generation rate of the hole-electron pairs at a depth z when light is incident perpendicular to the surface $z = 0$. We let $g(a - x)$ denote the generation rate for the vertical junction photoconverters when light is incident upon the face $x = a$. In equation (1), ϕ_0 in cm^{-2}-s^{-1} is the rate of incident photons per second per unit area, R is the fraction reflected from the surface, and α is the absorption coefficient in cm^{-1} at the wavelength considered.

Conventional Photoconverter

We consider first the model for a conventional planar photoconverter with light incident upon the face $z = 0$. For the region R_n, the diffusion of the excess carriers $p = p_n - p_{n_0}$ in the n-material is governed by the equation

$$H(p; L_p) = -g(z)/D_p \qquad (x, y, z \in R_n)$$

where

$$H(u; L_p) = \nabla^2 u - \frac{u}{L_p 2} \tag{2}$$

which is subject to the following boundary conditions:

$$\left.\begin{aligned} B(p; x; D_p) &= S_0 p & (x = a) \\ B(p; x; D_p) &= -S_0 p & (x = -a) \\ B(p; y; D_p) &= S_0 p & (y = b) \\ B(p; y; D_p) &= -S_0 p & (y = -b) \\ B(p; z; D_p) &= -S_p p & (z = 0) \\ p &= 0 & (z = z_j) \end{aligned}\right\} \tag{3}$$

with

$$B(u; x; c) = -c\frac{\partial u}{\partial x}$$

a boundary operator, and where c is a dummy parameter within the operator. The parameters in equations (2) and (3) are S_0, the surface recombination velocity at the sides; S_p, the surface recombination velocity at the surface $z = 0$; D_p, the diffusion coefficient of holes; and L_p, the diffusion length of holes in an average lifetime.

For the region R_p, the diffusion of the excess minority carriers $n = n_p - n_{p_0}$ in the p-material is governed by the equation

$$H(n; L_n) = \frac{-g(z)}{D_n} \qquad (x, y, z, \in R_p) \tag{4}$$

which is subject to the following boundary conditions:

$$\left.\begin{aligned} B(n; x; D_n) &= S_1 n & (x = a) \\ B(n; x; D_n) &= -S_1 n & (x = -a) \\ B(n; y; D_n) &= S_1 n & (y = b) \\ B(n; y; D_n) &= -S_1 n & (y = -b) \\ B(n; z; D_n) &= S_n n & (z = H) \\ n &= 0 & (z = z_j + \omega) \end{aligned}\right\} \tag{5}$$

with parameters S_1, the surface recombination velocity at the sides; S_n, the surface recombination velocity at the surface $z = H$; D_n, the diffusion coefficient of electrons; and L_n, the diffusion length of electrons.

Associated with the boundary value problem using equations (2) and (3) is a Green's function $G_1(x, y, z;\ x_0, y_0, z_0)$ which can be obtained by the method of separation of variables.

This enables us to represent the solution to the boundary value problem of equations (2) and (3) in the form:

$$p = p_n - p_{n_0} = \int_0^{z_j} \int_{-b}^{b} \int_{-a}^{a} \frac{-g(z_0)}{D_p} G_1(x, y, z; x_0, y_0, z_0)\, dx_0\, dy_0\, dz_0 \tag{6}$$

Similarly, there is a Green's function $G_2(x, y, z; x_0, y_0, z_0)$ associated with the boundary value problem using equations (4) and (5) which enables us to represent the solution to equations (4) and (5) in the form:

$$n = n_p - n_{p_0} = \int_{z_j+\omega}^{H} \int_{-b}^{b} \int_{-a}^{a} \frac{-g(z_0)}{D_n} G_2(x, y, z; x_0, y_0, z_0)\, dx_0\, dy_0\, dz_0 \tag{7}$$

The functions G_1 and G_2 can be expressed as a double Fourier series in terms of the eigenfunctions associated with the Sturm-Liouville problem (ref. 4):

$$\frac{d^2u}{dr^2} + \lambda^2 u = 0 \tag{8}$$

with the following boundary conditions:

$$B(u; r; D) = S_3 u \quad (r = h)$$
$$B(u; r; D) = S_3 u \quad (r = -h)$$

The eigenfunctions for this problem are given by

$$u_n = u(r; D, S_3, h, \lambda_n) = \cos\ \lambda_n r \tag{9}$$

where the eigenvalues λ_n satisfy the equation

$$\varsigma_n \tan\ \varsigma_n = \frac{S_3 h}{D} \quad (\varsigma_n = \lambda_n h)$$

Note that for large values of n, ς_{n+1} approaches $n\pi$. Also the eigenfunctions are orthogonal over the interval $(-h, h)$ with norm squared given by

$$\|u_n\|^2 = h + \frac{S_3 h^2}{D} \frac{\cos^2\ \varsigma_n}{\varsigma_n^2} \qquad (\varsigma_n = \lambda_n h) \tag{10}$$

We can then define the eigenfunction associates with the regions R_n and R_p as

$$\begin{aligned} U_m(x) &= u(x; D_p, S_0, a, \lambda_m) = \cos\ \lambda_m x \\ V_m(y) &= u(y; D_p, S_0, b, \eta_m) = \cos\ \eta_m y \\ U_m^*(x) &= U(x; D_n, S_1, a, \lambda_m^*) = \cos\ \lambda_m^* x \\ V_m^*(y) &= U(y; D_n, S_1, b, \eta_m^*) = \cos\ \eta_m^* y \end{aligned} \tag{11}$$

The Green's functions G_1 and G_2 can be represented in the form of a double Fourier series symmetric in x and y given by

$$G_1 = \sum_{i=1}^{\infty} \sum_{j=1}^{\infty} \frac{\psi_{1ij}}{\Delta_1} \frac{U_j(x_0)\, U_j(x)\, V_i(y_0)\, V_i(y)}{\|U_j\|^2\, \|V_i\|^2} \tag{12}$$

$$G_2 = \sum_{i=1}^{\infty}\sum_{j=1}^{\infty} \frac{\psi_{2ij}}{\Delta_2} \frac{U_j^*(x_0)\, U_j^*(x)\, V_i^*(y_0)\, V_i^*(y)}{\left\|U_j^*\right\|^2 \left\|V_i^*\right\|^2} \tag{13}$$

where

$$\psi_{1ij} = \begin{cases} Y_1(z_0)\, Y_2(z) & (0 < z_0 < z) \\ Y_1(z)\, Y_2(z_0) & (z < z_0 < z_j) \end{cases}$$

$$\psi_{2ij} = \begin{cases} Y_3(z_0)\, Y_4(z) & (z_j + \omega < z_0 < z) \\ Y_3(z)\, Y_4(z_0) & (z < z_0 < H) \end{cases} \tag{14}$$

$$\Delta_1 = \frac{-Y_1(z_j)}{\gamma_{ij} \sinh\left(z_j/\gamma_{ij}\right)}$$

$$\Delta_2 = \frac{Y_4(z_j + \omega)}{\sigma_{ij}}$$

with

$$Y_1(z) = \cosh\left(\frac{z}{\gamma_{ij}}\right) + \frac{S_p \gamma_{ij}}{D_p} \sinh\left(\frac{z}{\gamma_{ij}}\right)$$

$$Y_2(z) = \sinh \frac{\left[(z_j - z)/\gamma_{ij}\right]}{\sinh\left(z/\gamma_{ij}\right)} \tag{15}$$

$$Y_3(z) = \sinh\left[\frac{z - (z_j + \omega)}{\sigma_{ij}}\right]$$

$$Y_4(z) = \cosh\left(\frac{H - z}{\sigma_{ij}}\right) + \frac{S_n \sigma_{ij}}{D_n} \sinh\left(\frac{H - z}{\sigma_{ij}}\right)$$

having the parameters γ_{ij} and σ_{ij} defined by

$$\gamma_{ij}^2 = \frac{L_p^2}{1 + L_p^2(\lambda_i^2 + \eta_j^2)}$$

$$\sigma_{ij}^2 = \frac{L_n^2}{1 + L_n^2(\lambda_i^{*2} + \eta_j^{*2})}$$

From equations (6) and (7), we can obtain the current densities as follows:

$$J_p = -qD_p \frac{\partial(p_n - p_{n_0})}{\partial z} \qquad (z = z_j)$$

$$J_n = qD_n \frac{\partial(n_p - n_{p_0})}{\partial z} \quad (z = z_j + \omega) \tag{16}$$

This gives the total short circuit current $J_{sc} = J_p + J_n$.

By an analysis of Green's second formula, we can calculate the dark currents associated with the regions R_n and R_p. In the region R_n, we obtain a modification of the boundary value problem using equations (2) and (3). The modification being that in equation (2), we let $g = 0$, and in equation (3), we require that

$$p_n - p_{n_0} = p_{n_0}\left[\exp\left(\frac{qV_j}{KT}\right) - 1\right] \qquad (z = z_j)$$

where V_j is the junction voltage. This boundary value problem has the solution

$$p_n - p_{n_0} = \int_{-b}^{b}\int_{-a}^{a} p_{n_0}\left[\exp\left(\frac{qV_j}{KT}\right) - 1\right]\left.\frac{\partial G_1}{\partial z_0}\right|_{z_0=z_j} dx_0\, dy_0 \tag{17}$$

from which we can obtain the dark current opposing the photocurrent as

$$J_{pd} = -qD_p \text{ grad } (p_n - p_{n_0}) \cdot \hat{k} \qquad (z = z_j) \tag{18}$$

Similarly, in the region R_p, we obtain for the model of the dark current a modification of the boundary value problem with equations (4) and (5). The modification being that in equation (4), $g = 0$, and in equations (5), we require that

$$n_p - n_{p_0} = \left[\exp\left(\frac{qV_j}{KT}\right) - 1\right] \qquad (z = z_j + \omega)$$

This boundary value problem has the solution

$$n_p - n_{p_0} = \int_{-b}^{b}\int_{-a}^{a} n_{p_0}\left[\exp\left(\frac{qV_j}{KT}\right) - 1\right]\left.\frac{\partial G_2}{\partial z_0}\right|_{z_0=z_j+\omega} dx_0\, dy_0 \tag{19}$$

which, in turn, produces the dark current

$$J_{nd} = -qD_n \text{ grad } (n_p - n_{p_0}) \cdot (-\hat{k}) \qquad (z = z_j + \omega) \tag{20}$$

The total dark current is then a summation of the results in equations (18) and (20) and we obtain

$$J_d = J_{pd} + J_{nd} = J_0\left[\exp\left(\frac{qV_j}{KT}\right) - 1\right] \tag{21}$$

We use the recombination current density J_{rec} from reference 4 and calculate the total current by integration with respect to x and y over a plane represented by z = Constant.

The current-voltage relation is obtained from the equation relating the current and voltage for the equivalent circuit diagram of figure 2 and we find

$$I\left(1 + \frac{R_s}{R_{sh}}\right) = I_{sc} - \frac{V}{R_{sh}} - I_d$$

where R_s is the series resistance and R_{sh} is the shunt resistance.

Vertical Junction Photoconverter

For the vertical junction photoconverter, we assume that light is incident upon the face $x = a$. In the boundary value problems using equations (2), (3), (4), and (5), the generation term $g(z)$ is replaced by $g(a - x)$. Also in equations (6) and (7), the form of the double Fourier series representing the Green's function must be changed because in the vertical junction case

we no longer have symmetry in the x-direction. We consider the following Sturm-Liouville problems (SLP) in the regions R_n and R_p. In the region R_n, we consider

$$L(W) = W'' + \eta^2 W = 0 \qquad (0 < z < z_j) \tag{22}$$

subject to the boundary conditions

$$\begin{aligned} W &= 0 \qquad (z = z_j) \\ B(W; z, D_p) &= -S_p W \qquad (z = 0) \end{aligned}$$

In the region R_p we consider the SLP

$$L(W^*) = W^{*\prime\prime} + \eta^2 W^* = 0 \qquad (z_j + \omega < z < h) \tag{23}$$

subject to the boundary conditions

$$\begin{aligned} W^* &= 0 \quad (z = z_j + \omega) \\ B(W^*; z, D_n) &= S_n W^* \quad (z = H) \end{aligned}$$

The eigenvalues of the SLP in equation (22) satisfy

$$\frac{-D_p(\eta_i z_j)}{S_p z_j} = \tan\ \eta_i z_j \quad (i = 1,\ 2,\ 3,\ \ldots) \tag{24}$$

and the eigenvalues of the SLP in equation (23) satisfy

$$\frac{-D_n(\eta_i^* h')}{S_n h'} = \tan\ \eta_i^* h' \quad (i = 1,\ 2,\ 3,\ \ldots) \tag{25}$$

with $h' = H - z_j - \omega$. The corresponding eigenfunctions for the regions R_n and R_p are, respectively,

$$W_i(z) = \sin\ \eta_i(z_j - z) \quad (i = 1,\ 2,\ 3,\ \ldots) \tag{26}$$

and

$$W_i^*(z) = \sin\ \eta_i^*(z - z_j - \omega) \quad (i = 1,\ 2,\ 3,\ \ldots) \tag{27}$$

which have the square norms

$$\|W_i\|^2 = \frac{1}{2} z_j - \frac{1}{4} \frac{\sin\ 2\eta_i z_j}{\eta_i} \quad (i = 1,\ 2,\ 3,\ \ldots) \tag{28}$$

$$\|W_i^*\|^2 = \frac{1}{2} h' - \frac{1}{4} \frac{\sin\ 2\eta_i^* h'}{\eta_i^*} \quad (i = 1,\ 2,\ 3,\ \ldots) \tag{29}$$

For the vertical junction case, the Green's functions for the regions R_n and R_p are represented as the double Fourier series

$$g_1(x, y, z; x_0, y_0, z_0) = \sum_{i=1}^{\infty} \sum_{j=1}^{\infty} \frac{V_i(y)\ W_j(z)\ V_i(y_0)\ W_j(z_0)\ \psi_{3ij}}{\|V_i\|^2 \|W_j\|^2 \rho_{ij}} \tag{30}$$

$$g_2(x, y, z; x_0, y_0, z_0) = \sum_{i=1}^{\infty} \sum_{j=1}^{\infty} \frac{V_i^*(y)\ W_j^*(z)\ V_i^*(y_0)\ W_j^*(z_0)\ \psi_{4ij}}{\|V_i^*\|^2 \|W_j^*\|^2 \rho_{ij}^*} \tag{31}$$

where V_i^* and V_i have been previously defined in equation (11). The remaining terms in equations (30) and (31) are determined from the relations:

$$\psi_{3ij} = \left\{ \begin{array}{ll} -Y_1(x)\ Y_2(x_0) & (-a \leq x_0 < x) \\ -Y_1(x_0)\ Y_2(x) & (x < x_0 \leq a) \end{array} \right\}$$

$$\psi_{4ij} = \left\{ \begin{array}{ll} -Y_3(x)\ Y_4(x_0) & (-a \leq x_0 < x) \\ -Y_3(x_0)\ Y_4(x) & (x < x_0 \leq a) \end{array} \right\}$$

$$\begin{aligned} Y_1(x) &= F_1(x; \Gamma_{ij}, S_0, D_p) \\ Y_2(x) &= Y_1(-x) \\ Y_3(x) &= F_1(x; \varepsilon_{ij}, S_1, D_n) \\ Y_4(x) &= Y_3(-x) \end{aligned}$$

$$F_1(x; A, B, C) = \cosh\left(\frac{a-x}{A}\right) + \frac{AB}{C}\ \sinh\left(\frac{a-x}{A}\right)$$

$$\begin{aligned} \Gamma_{ij}^2 &= \frac{L_p^2}{1 + L_p^2\left(\mu_i^2 + \eta_j^2\right)} \\ \varepsilon_{ij}^2 &= \frac{L_n^2}{1 + L_n^2\left(\mu_i^{*2} + \eta_j^{*2}\right)} \\ \rho_{ij} &= F_2\left(\Gamma_{ij}, S_0, D_p\right) \\ \rho_{ij}^* &= F_2\left(\varepsilon_{ij}, S_1, D_n\right) \end{aligned}$$

$$F_2(A, B, C) = \left(\frac{1}{A} + \frac{B^2 A}{C^2}\right)\ \sinh\left(\frac{2a}{A}\right) + \frac{2B}{C}\ \cosh\left(\frac{2a}{A}\right)$$

In equations (2) and (3), we replace $g(z)$ by $g(a-x)$, then in the region R_n the density of excess minority carriers can be represented in the form

$$p_n - p_{n_0} = \int_0^{z_j} \int_{-b}^{b} \int_{-a}^{a} \frac{g(a-x_0)}{D_p} g_1(x, y, z; x_0, y_0, z_0)\ dx_0\ dy_0\ dz_0$$

Similarly in equations (4) and (5), we replace $g(z)$ by $g(a-x)$ and find that the solution for the excess minority carriers in the region R_p can be represented in the form

$$n_p - n_{p_0} = \int_{z_j+\omega}^{h} \int_{-b}^{b} \int_{-a}^{a} -\frac{g(a-x_0)}{D_n} g_2(x, y, z; y_0, z_0)\ dx_0\ dy_0\ dz_0$$

With the photocurrent relations of equation (18), we can produce the photocurrent responses at the junction edges z_j and $z_j + \omega$ from which we can calculate the total short circuit current.

Computer programs simulating both the conventional and vertical junction photoconverter responses have been developed. As a check on the results obtained from these three-dimensional models, we constructed one-dimensional models of both the conventional and vertical junction photoconverters, and the results from that study can be found in reference 5.

Results and Discussion

Comparison of Conventional and Vertical Junction Converters

Figure 3 gives the efficiencies of a conventional converter and a vertical junction converter for Nd laser radiation. These efficiencies were calculated by using the nominal parameters shown in table I. The efficiency of the vertical junction converter at an input power of 1 kW-cm^{-2} is 47 percent, whereas under the same conditions, the efficiency of the conventional converter is only 17 percent. Because of the higher efficiency of the vertical junction converter, a detailed parametric study has been done for this converter.

Parametric Study of Vertical Junction Converters

Since the efficiency of the vertical junction converter is significantly higher than the efficiency of the conventional converter, a parametric study of the vertical junction converter has been done. Baseline parameters shown in table II were assigned individually to determine the optimum, achievable value for each parameter. The best set of these values was then assigned to describe the optimum vertical junction converter for use with a 1.06-μm Nd laser.

Application of Model to Si Vertical Junction Converter Nd Laser System

It has been shown previously that Si vertical junction converters are appropriate for use with a Nd laser to form a space power system (refs. 2 and 5). We have applied our three-dimensional model for vertical junction converters to such a system. The effects of various design parameters are shown, and the optimum single junction converter is described.

The set of converter baseline parameters chosen is shown in table II. These parameters were varied individually in order to determine their optimum values and then assembled to describe the optimum single junction converter. Each parameter is discussed separately.

Carrier Concentration

Figure 4 shows the effect of carrier concentration on converter efficiency for our baseline conditions. The peak baseline efficiency of 47.5 percent occurs at an acceptor concentration of 1×10^{18} carriers-cm^{-3}. The peak baseline efficiency of 51.2 percent occurs at a donor concentration of 1×10^{18} carriers-cm^{-3}. We chose for our optimum carrier concentrations both donor and acceptor concentrations of 1×10^{18} carriers-cm^{-3}.

Converter depth. Figure 5 shows the effect of converter depth on converter efficiency. The efficiency increases from 20.5 percent at a depth of 5 μm to 47.8 percent at a depth of 35 μm. We have taken 35 μm as the optimum converter depth.

Converter thickness. Figure 6 shows the effect of converter thickness on converter efficiency. The efficiency increases to a maximum baseline efficiency of 45.5 percent at a converter thickness of 1000 μm. This thickness of 1000 μm is used as the thickness of our optimum converter.

Junction position. Figure 7 shows the effect of junction position on converter efficiency. As the depth of the n-layer (junction position) decreases, the converter efficiency increases. From a fabrication consideration, we have chosen 2 μm as a practical, achievable junction position for our optimum converter. The peak baseline efficiency is 51.2 percent.

Series resistance. Figure 8 shows the effect of series resistance on the converter efficiency. The efficiency decreases from 45.5 percent at 0.1 mΩ to 7.7 percent at a series resistance of 1 ohm. For our optimum converter, we have chosen a series resistance of 1 mΩ corresponding to 20 μm of silicon thickness. The baseline efficiency with this series resistance is 45.4 percent.

Temperature. Figure 9 shows the converter efficiency as a function of temperature. Note that the efficiency decreases with increasing temperature. The efficiency at our operating temperature of 300 K is 45.4 percent. Operation of Si above 500 K may not be practical.

Surface recombination velocity. Figure 10 shows the effect of n-surface recombination velocity and p-surface recombination velocity on converter efficiency. As the n-surface recombination velocity increases from 0.01 m-sec^{-1} to 100 m-sec^{-1}, the efficiency decreases from 49.4 percent to 31.1 percent. As the p-surface recombination velocity increases from 0.01 m-sec^{-1} to 100 m-sec^{-1}, the efficiency decreases from 47.6 percent to 38.7 percent. According to reference 6, a surface recombination velocity of 1 m-sec^{-1} is achievable in Si; therefore, we have chosen 1 m-sec^{-1} as the recombination velocity of our optimum, achievable converter. The baseline efficiency at this surface recombination velocity is 45.5 percent.

Optimum converter. From this parametric study, a set of optimum parameters has been determined. These are shown in table III. The efficiency of the optimum converter is 43.9 percent at 1 kW-cm^{-2}. Specific results from this computer study were presented in graphical form to illustrate the importance of the parameter changes. Major factors to consider in the design of an efficient vertical junction, high-intensity photoconverter are the surface recombination velocity and the series resistance. Figure 11 shows the converter efficiency as a function of input power for the optimized vertical junction converter. The efficiency varies from 33 percent at 1 kW-cm^{-2} to 44 percent at 1 kW-cm^{-2}.

Concluding Remarks

We have presented a three-dimensional model for the analysis of a conventional and a vertical junction photoconverter for the conversion of laser power into electrical power. The model requires the representation of Green's functions in the form of a double Fourier series. A set of nominal values was assigned to the parameters in the model, and then a comparison of the conventional and vertical junction photoconverter was undertaken. The calculated efficiency of the vertical junction converter is 47 percent, whereas the calculated efficiency of the conventional converter is 17 percent. A parametric study of the higher efficiency vertical junction converter has been done. The efficiency at 1 kW-cm^{-2} for our optimized converter is 44 percent.

NASA Langley Research Center
Hampton, Virginia 23665-5225
May 3, 1988

References

1. DeYoung, R. J.; Tepper, W. D.; Conway, E. J.; and Humes, D. H.: Preliminary Comparison of Laser and Solar Space Power Systems. *18th Intersociety Energy Conversion Engineering Conference, Volume 3—Electrical Power Systems,* American Inst. of Chemical Engineers, c.1983, pp. 983–989.
2. Walker, Gilbert H.: Photovoltaic Conversion of Laser to Electrical Power. *18th Intersociety Energy Conversion Engineering Conference, Volume 3—Electrical Power Systems,* American Inst. of Chemical Engineers, c.1983, pp. 1194–1199.
3. Stakgold, Ivar: *Green's Functions and Boundary Value Problems.* John Wiley & Sons, Inc., c.1979.
4. Halder, N. C.; and Williams, T. R.: Grain Boundary Effects in Polycrystalline Silicon Cells. I: Solution of the Three-Dimensional Diffusion Equation by the Green's Function Method. *Sol. Cells,* vol. 8, no. 3, Apr. 1983, pp. 201–223.
5. Walker, G. H.; and Heinbockel, J. H.: Parametric Study of Laser Photovoltaic Energy Converters. *Sol. Cells,* vol. 22, no. 1, Sept. 1987, pp. 55–67.
6. Hovel, Harold J.: *Semiconductors and Semimetals. Volume 11—Solar Cells.* Academic Press, Inc., 1975.

Table I. Nominal Values Used in Initial Calculations

Parameter	Conventional	Vertical junction
Dimensions (see fig. 1):		
Thickness, a, mm	5	5
Width, b, mm	5	5
Junction depth, z_j, μm	5	20
Mobility for—		
Region n, $cm^2\text{-}V^{-1}\text{-}s^{-1}$	711.3	711.3
Region p, $cm^2\text{-}V^{-1}\text{-}s^{-1}$	89.7	89.7
Laser wavelength, μm	1.06	1.06
Surface recombination velocity on—		
Surface n, $cm\text{-}s^{-1}$	1.0	1.0
Surface p, $cm\text{-}s^{-1}$	1.0	1.0
Series resistance, Ω	0	0
Shunt resistance, Ω	1.0×10^6	1.0×10^6
Doping density for—		
Na (acceptor), cm^{-3}	1.25×10^{17}	1.25×10^{17}
Nd (donor), cm^{-3}	5.0×10^{19}	5.0×10^{19}
Lifetime for—		
Region n, s	10.0×10^{-4}	10.0×10^{-4}
Region p, s	5.0×10^{-5}	5.0×10^{-5}
Laser power, $kW\text{-}cm^{-2}$	1.0	1.0
Temperature, K	293	293

Table II. Baseline Parameters Used for Vertical Junction Case Parametric Study

Laser power, kW-cm^{-2}	1
Laser wavelength, μm	1.06
Dimensions (see fig. 1):	
Thickness, a, mm	0.65
Width, b, mm	5
Depth, H, mm	0.02
Junction position, μm	10
Surface recombination velocity on—	
Surface n, cm-s^{-1}	1.0×10^3
Surface p, cm-s^{-1}	1.0×10^3
Series resistance, Ω	0
Shunt resistance, Ω	1.0×10^6
Doping density for—	
Na (acceptor), cm^{-3}	1.25×10^{17}
Nd (donor), cm^{-3}	5.0×10^{19}
Mobility for—	
Region n, cm^2-V^{-1}-s^{-1}	711.3
Region p, cm^2-V^{-1}-s^{-1}	89.7
Lifetime for—	
Region n, s	1.0×10^{-3}
Region p, s	5×10^{-5}
Temperature, K	300

Table III. Parameters for Optimum Converter

Laser power, kW-cm^{-2}	1
Laser wavelength, μm	1.06
Dimensions (see fig. 1):	
Thickness, a, mm	1000
Width, b, mm	5
Depth, H, mm	35
Junction position, μm	20
Surface recombination velocity on—	
Surface n, m-s^{-1}	1
Surface p, m-s^{-1}	1
Series resistance, Ω	0.001
Shunt resistance, Ω	1×10^6
Doping density for—	
Acceptors, cm^{-3}	1×10^{18}
Donors, cm^{-3}	1×10^{18}
Temperature, K	300

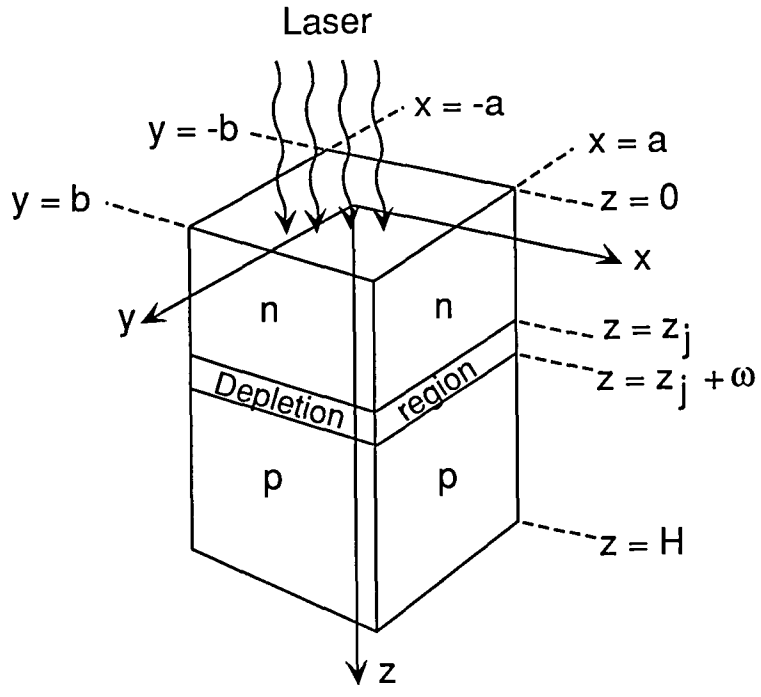

(a) Conventional converter.

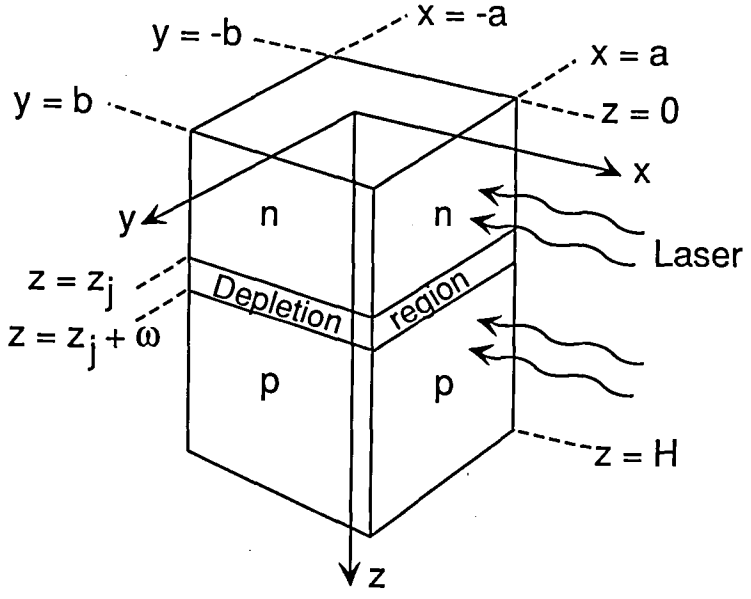

(b) Vertical converter.

Figure 1. Geometry for three-dimensional model.

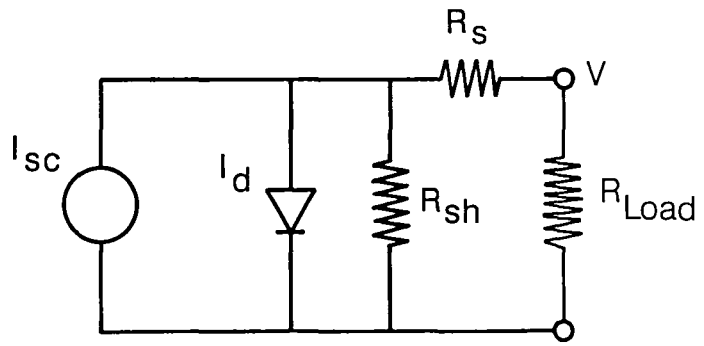

Figure 2. Equivalent circuit diagram.

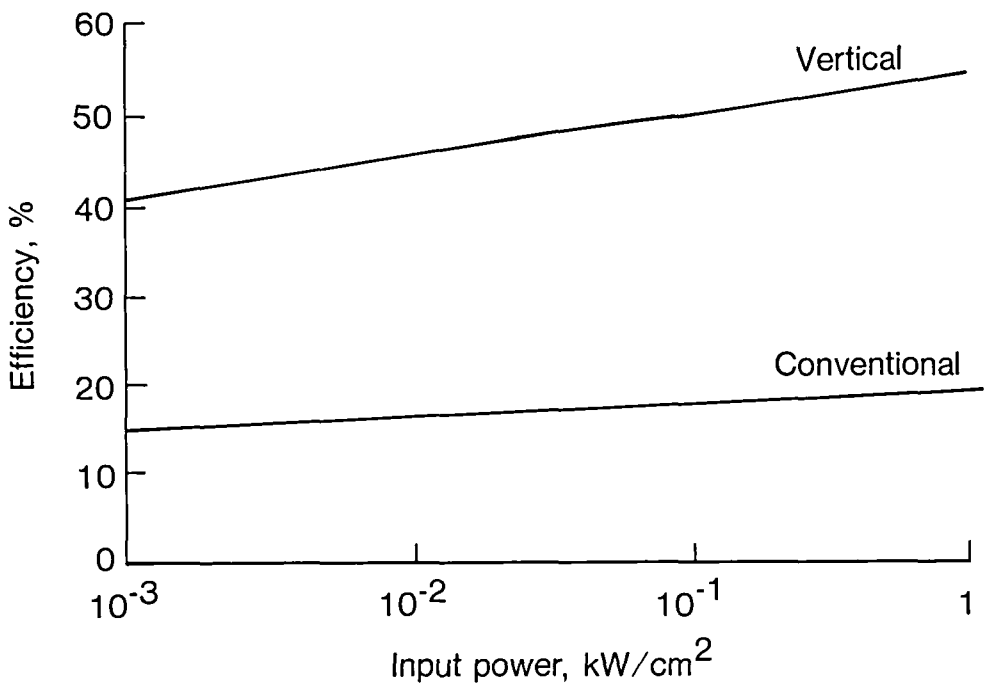

Figure 3. Efficiency versus input power for conventional and vertical junction converters.

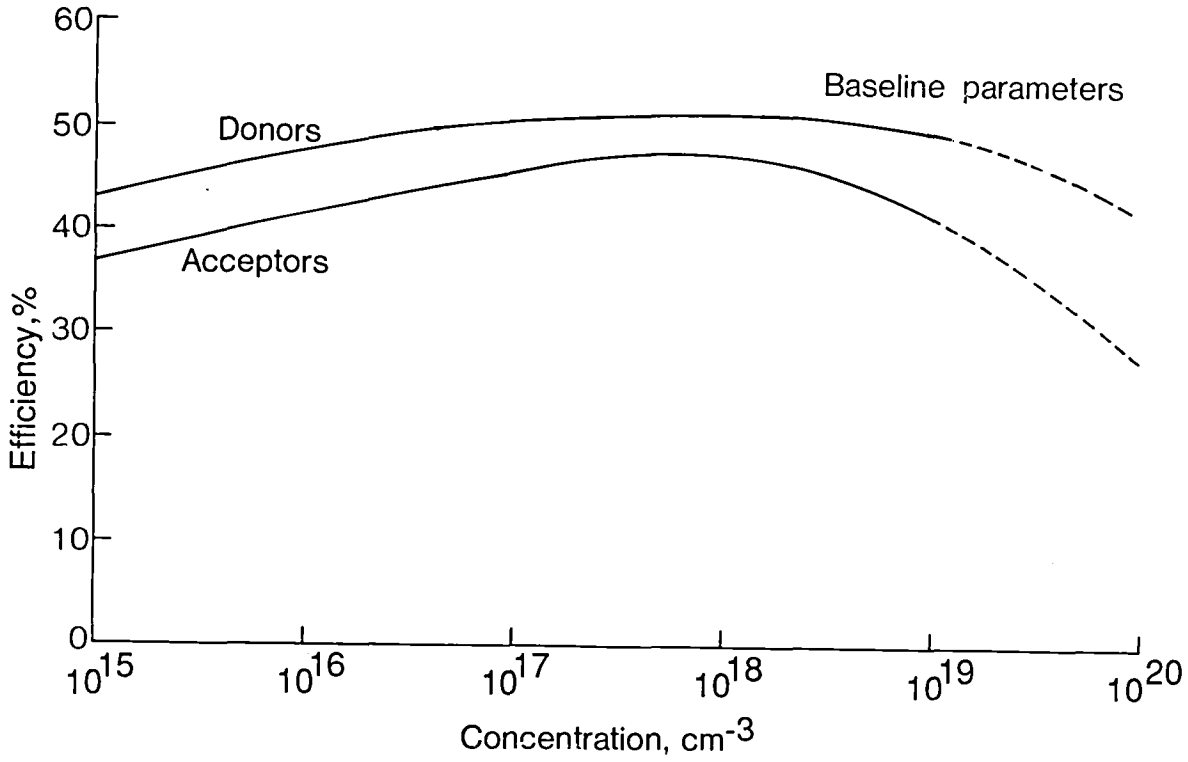

Figure 4. Efficiency versus acceptor and donor concentration for vertical junction converter under baseline conditions.

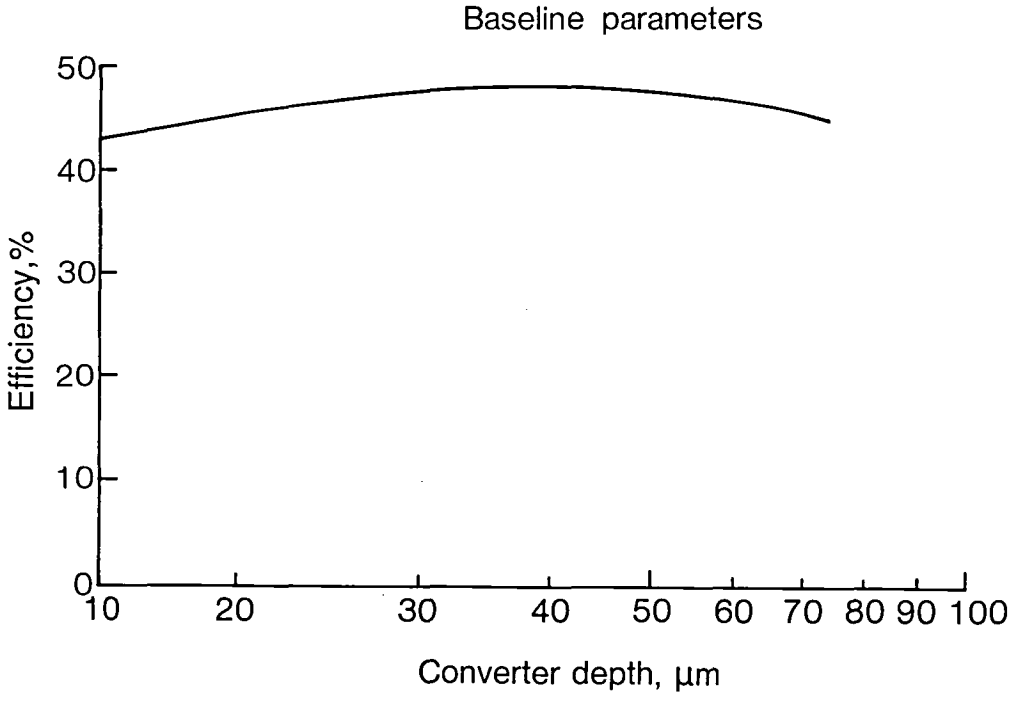

Figure 5. Efficiency versus converter depth for vertical junction converter under baseline conditions.

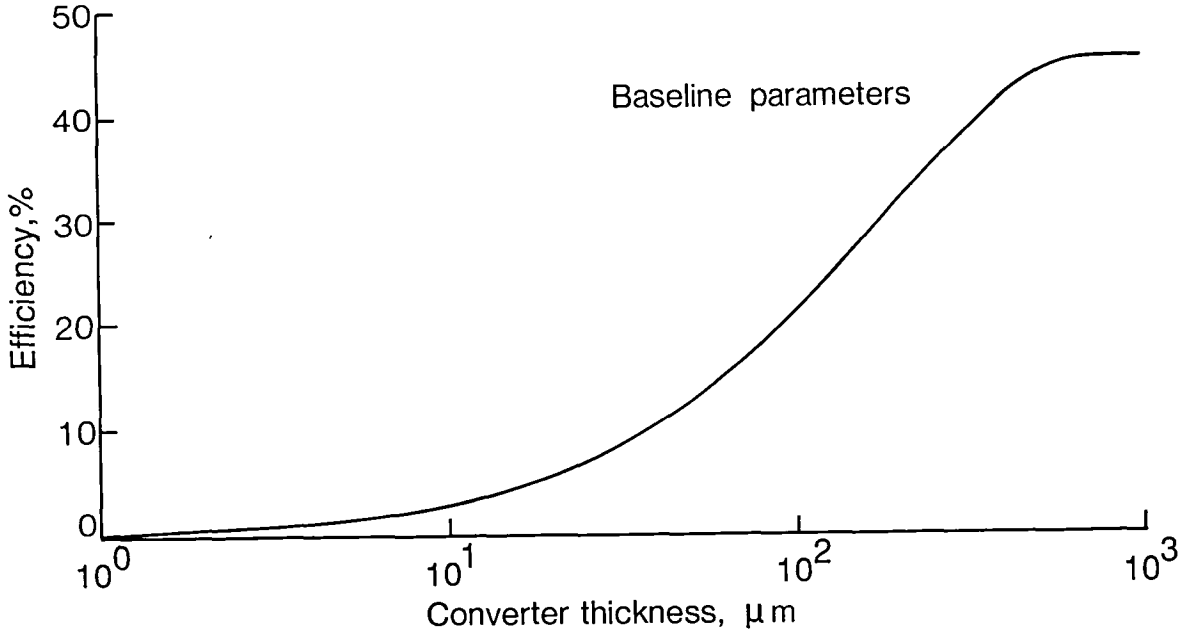

Figure 6. Efficiency versus converter thickness under baseline conditions.

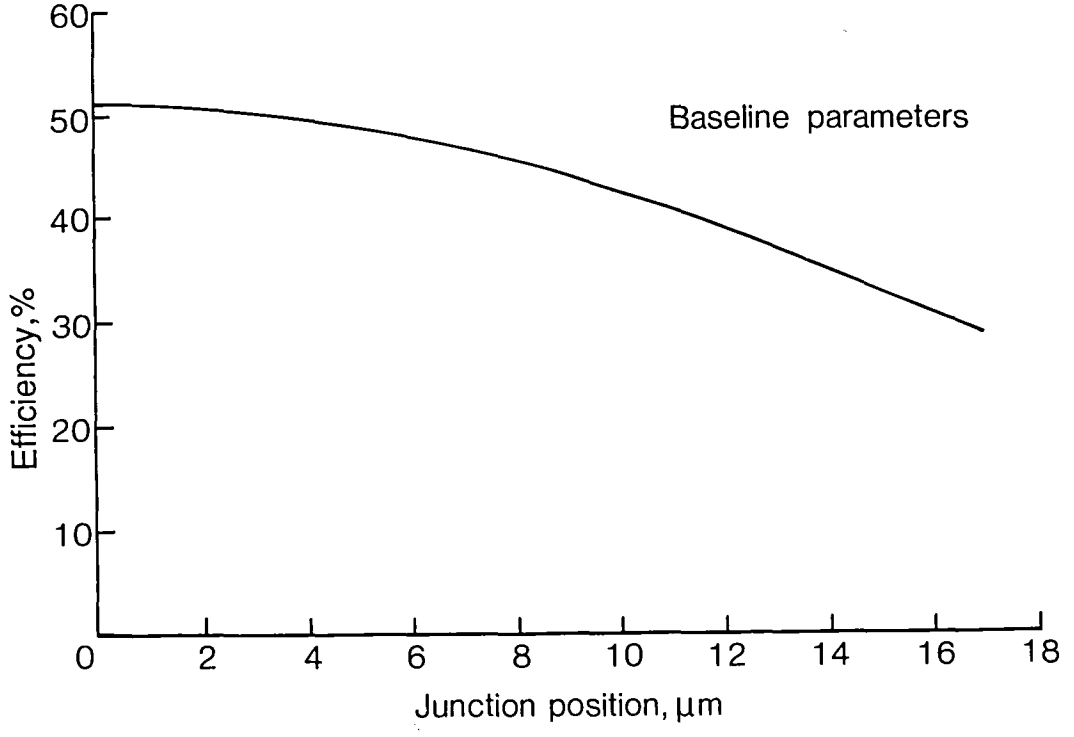

Figure 7. Efficiency versus junction position for vertical junction converter under baseline conditions.

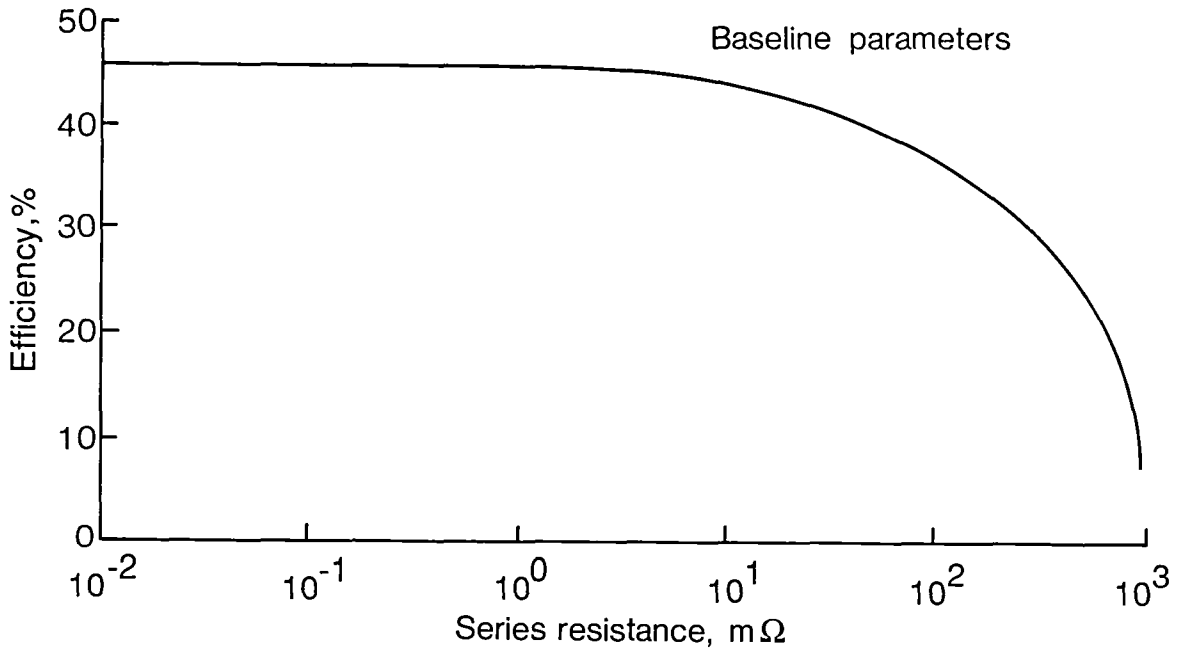

Figure 8. Efficiency versus series resistance for vertical junction converter under baseline conditions.

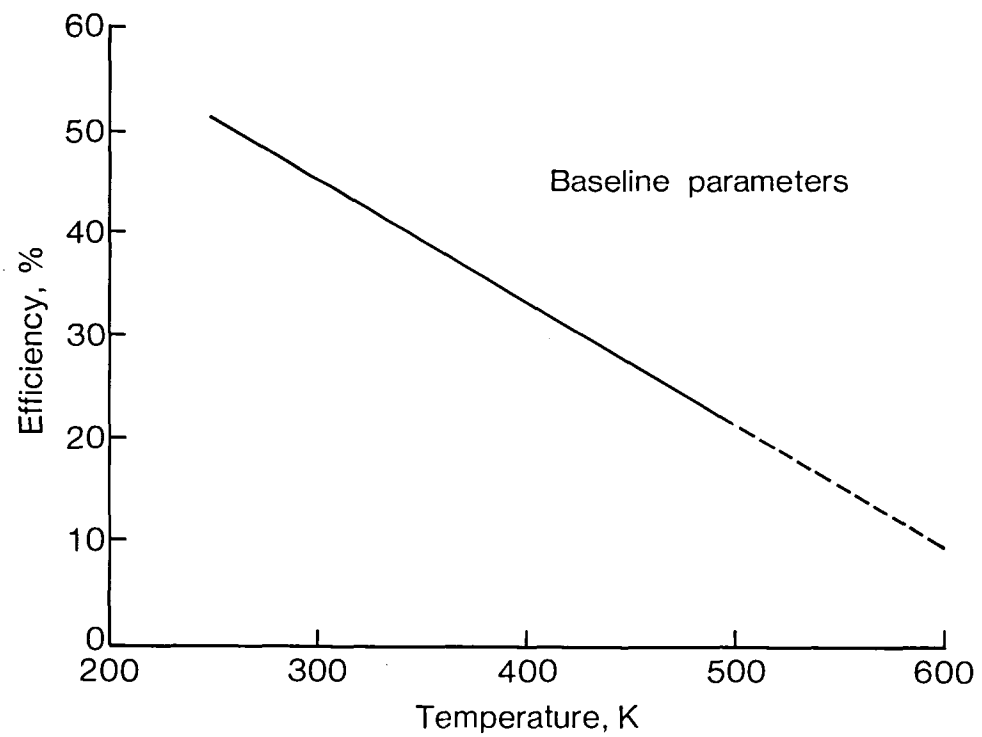

Figure 9. Efficiency versus temperature for a vertical junction converter under baseline conditions.

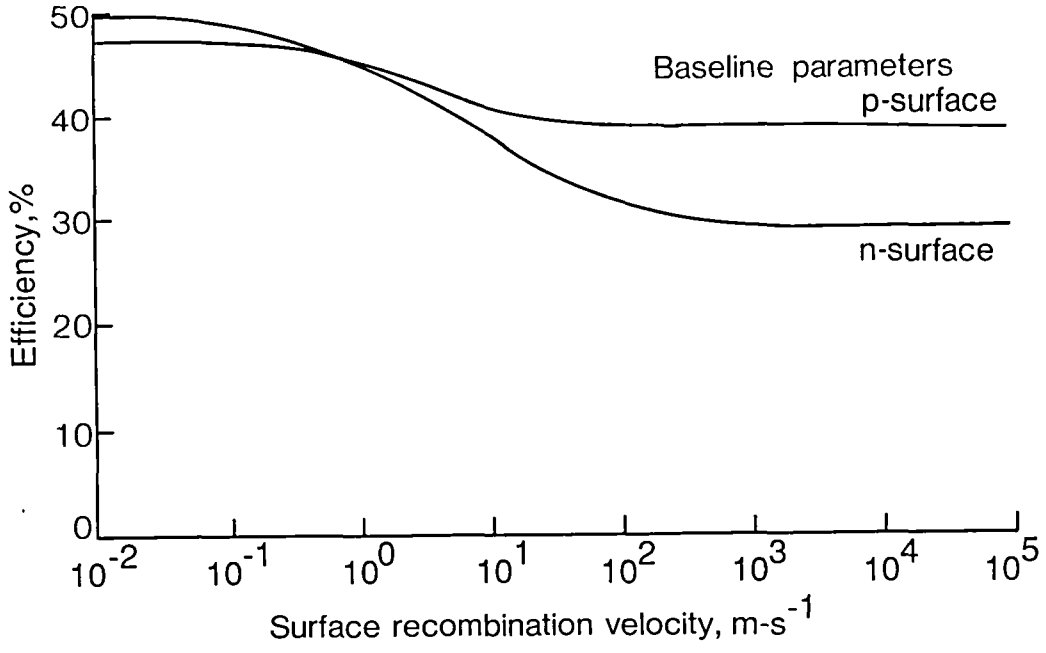

Figure 10. Efficiency versus n-surface recombination velocity and p-surface recombination velocity under baseline conditions.

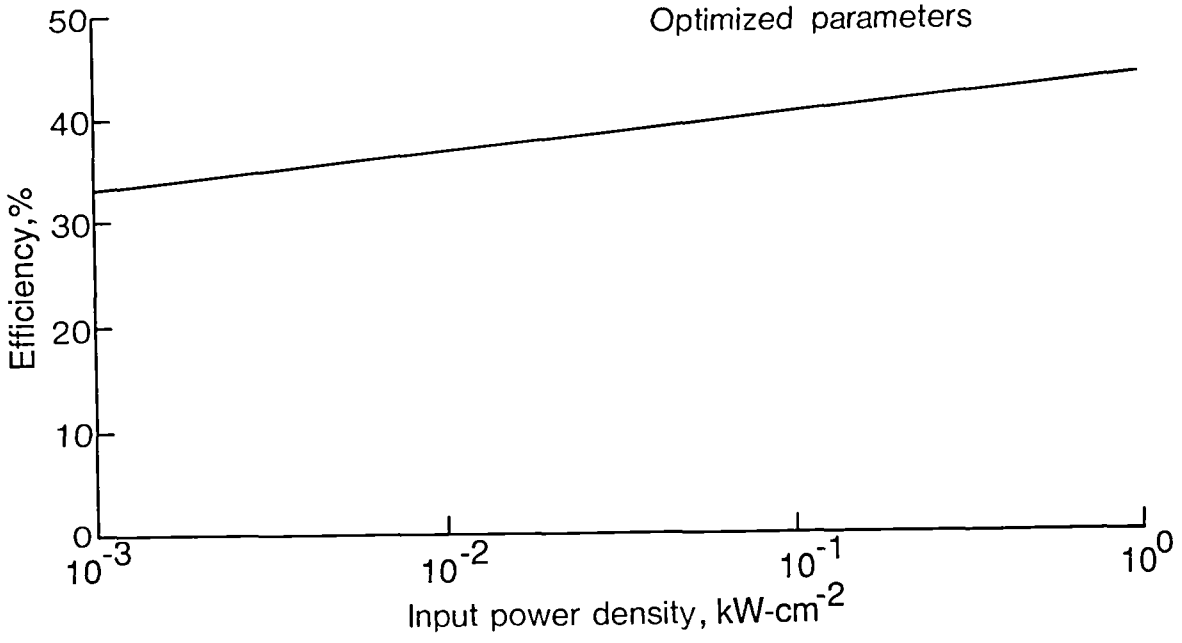

Figure 11. Efficiency versus input power density for optimized vertical junction converter.

NASA
National Aeronautics and Space Administration

Report Documentation Page

1. Report No.	2. Government Accession No.	3. Recipient's Catalog No.
NASA TM-4039		

4. Title and Subtitle	5. Report Date
Three-Dimensional Models of Conventional and Vertical Junction Laser-Photovoltaic Energy Converters	July 1988
	6. Performing Organization Code
7. Author(s)	8. Performing Organization Report No.
John H. Heinbockel and Gilbert H. Walker	L-16424
9. Performing Organization Name and Address	10. Work Unit No.
NASA Langley Research Center Hampton, VA 23665-5225	506-41-41-01
	11. Contract or Grant No.
12. Sponsoring Agency Name and Address	13. Type of Report and Period Covered
National Aeronautics and Space Administration Washington, DC 20546-0001	Technical Memorandum
	14. Sponsoring Agency Code

15. Supplementary Notes

John H. Heinbockel: Old Dominion University, Norfolk, Virginia.
Gilbert H. Walker: Langley Research Center, Hampton, Virginia.

This research was supported in part by NASA Grant NAG1-148 with Old Dominion University Resesarch Foundation.

16. Abstract

Three-dimensional analytical models of both conventional planar junction and vertical junction photovoltaic energy converters have been constructed. The models are a set of linear partial differential equations and take into account many photoconverter design parameters. The model is applied to Si photoconverters; however, the model may be used with other semiconductors. When used with a Nd laser, the conversion efficiency of the Si vertical junction photoconverter is 47 percent, whereas the efficiency for the conventional planar Si photoconverter is only 17 percent. A parametric study of the Si vertical junction photoconverter is then done in order to describe the optimum converter for use with the 1.06-μm Nd laser. The efficiency of this optimized vertical junction converter is 44 percent at 1 kW-cm^{-2}.

17. Key Words (Suggested by Authors(s))	18. Distribution Statement
Energy conversion Photovoltaic converters Laser energy conversion Solid-state devices	Unclassified—Unlimited Subject Category 44

19. Security Classif.(of this report)	20. Security Classif.(of this page)	21. No. of Pages	22. Price
Unclassified	Unclassified	20	A02

National Aeronautics and
Space Administration
Code NTT-4

Washington, D.C.
20546-0001